Progress in Oceanography 228 (2024) 103316

Contents lists available at ScienceDirect

Progress in Oceanography

journal homepage: www.elsevier.com/locate/pocean

Constraining the twilight zone remineralization in the South China Sea basin: Insights from the multi-method intercomparison

Chao Xu [a,b], Mingwang Xiang [a,b,c], Bingzhang Chen [d], Yibin Huang [a,*], Guoqiang Qiu [a], Yuchen Zhang [a,b], Haili Wang [a], Bangqin Huang [a,b,*]

[a] State Key Laboratory of Marine Environmental Science, Xiamen University, Xiamen, China
[b] Fujian Provincial Key Laboratory of Coastal Ecology and Environmental Studies, College of the Environment and Ecology, Xiamen University, Xiamen, China
[c] Guangxi Key Laboratory of Beibu Gulf Marine Resources, Environment and Sustainable Development, Fourth Institute of Oceanography, Ministry of Natural Resources, Beihai, China
[d] Department of Mathematics and Statistics, University of Strathclyde, Glasgow, UK

ARTICLE INFO

Keywords:
Twilight zone
Mesopelagic respiration
Carbon budget
South China Sea
Multi-method intercomparison

ABSTRACT

The twilight zone remineralization (TZR) consumes over 70% of organic carbon exported from the sunlit ocean, significantly affecting oceanic carbon sequestration and atmospheric CO_2 concentration. Despite the well-established importance, the quantification of TZR remains challenging, as reflected by conspicuous methodological discrepancy and the unsolved imbalance between carbon supply from the upper layer and demand at depth. Here we combined three independent approaches, including biogeochemical profiling floats (BGC-float) observation, *in vivo* reduction of the tetrazolium salt by the cellular electron transport system (*in vivo* INT), and the synthesis of prokaryotic respiration (PR) determined by radiolabeled leucine incorporation and zooplankton respiration (ZR) empirically estimated from the biomass (PR + ZR), to investigate the TZR in the South China Sea basin. Our results show that the BGC-float and PR + ZR approaches gave more consistent results, with the respective values of 5.1 ± 0.5 and 6.4 ± 3.0 mol C m^{-2} yr^{-1}. However, *in vivo* INT approach yielded a TZR nearly an order of magnitude higher at 30.0 ± 6.1 mol C m^{-2} yr^{-1}. To further reconcile methodological discrepancies, we estimated the possible range of carbon supply by integrating comprehensive carbon sources, including sinking particles, dissolved organic carbon input, lateral transport, dark carbon fixation, and active carbon transport by zooplankton migration. After considering multiple carbon sources, we successfully balanced the carbon demand as indicated by BGC-float and PR + ZR approaches. Our intercomparison exercise suggests a potential overestimation of TZR by the *in vivo* INT approach, and also highlights the importance of integrating multiple carbon sources in closing the twilight zone carbon budget.

1. Introduction

The biologically-mediated carbon production and its subsequent export to the deep ocean, a.k.a. biological carbon pump, is a key mechanism sustaining ocean carbon sequestration and greatly influences atmospheric CO_2 concentration (Boyd et al. 2019; Buesseler et al. 2020). The global carbon export at the base of the euphotic zone (typically defined as the 1% surface light) is presently estimated in an order of 5 to 12 Pg C yr^{-1} (Laws et al. 2011; Boyd et al. 2019; Buesseler et al. 2020), of which 60–80% is further consumed by heterotrophic organism in the twilight zone (typically defined as the depth between the base of the euphotic zone and 1000 m) (Henson et al. 2012; Giering et al. 2014). Thus, accurate quantification of twilight zone remineralization (TZR) is critical in understanding carbon transfer in the ocean interior and the amount of carbon that is ultimately buried in the seafloor, isolated from the atmosphere at the time scale of centuries to millennia (Chisholm 2000; Boyd et al. 2019).

The main approaches to quantify TZR can be broadly classified into two categories: incubation-based and incubation-free techniques. The most traditional incubation-based approach involves monitoring the oxygen consumption in the incubation bottle (Gaarder 1927; Ducklow and Doney 2013). However, this approach necessitates extended incubation periods (>24 h) to amplify the respiration signal, due to limited precision in traditional oxygen measurement. The long incubation

* Corresponding authors at: State Key Laboratory of Marine Environmental Science, Xiamen University, Xiamen, China.
E-mail addresses: yibin.huang@xmu.edu.cn (Y. Huang), bqhuang@xmu.edu.cn (B. Huang).

https://doi.org/10.1016/j.pocean.2024.103316
Received 1 December 2023; Received in revised form 17 June 2024; Accepted 23 July 2024
Available online 25 July 2024

presumably leads to an artificial modification in microbial community structure and trophic interactions during the incubation (del Giorgio and Williams 2005; Huang et al. 2019a). Fortunately, this drawback has been partially addressed with the recent advent of STOX electrodes (Tiano et al., 2014). These electrodes have significantly elevated the precision of O_2 measurement, allowing us to detect lower rates of respiration in shorter incubation periods. Alternatively, tracking respiration-relevant elements, such as the reduction of a tetrazolium salt by the cellular electron transport system (*in vitro* INT or *in vivo* INT) (Martínez-García et al., 2009), or radiolabeled leucine incorporation (a proxy of prokaryotic production activity that can be combined with growth efficiency rate to estimate prokaryotic respiration) (del Giorgio and Cole 1998; Steinberg et al. 2008; Shen et al. 2020), has gained popularity because of their high sensitivity. Although these approaches can circumvent long-term incubation, the common caveat of the incubation-based approaches is difficulty in simulating the deep environment, particularly the hydrostatic pressure and turbulence conditions (Martínez-García et al., 2009; Huang et al. 2019a; Amano et al. 2022; Guo et al. 2022). Non-incubation techniques to constrain TZR include using the mass balance model or the inert gas (e.g., Ar, Cassar et al. 2021) to isolate the physically-induced oxygen signal from the seawater chemical tracers change. Particularly, the recent advances in autonomous platforms (e.g., biogeochemical profiling floats (BGC-float) and Seagliders) and biogeochemical sensors development enable ocean biogeochemistry to be sampled at finer spatiotemporal scales (Chai et al. 2020; Claustre et al. 2020), providing a new means to resolving the TZR over the multiple time scales (Hennon et al., 2016). The accuracy of the tracer budget approach in TZR estimates mainly depends on the degree to which abiotic processes can be constrained (Hennon et al. 2016; Billheimer et al. 2021). Additionally, TZR can be empirically inferred from the biomass (Ikeda 1985; Ikeda et al. 2001; Steinberg et al. 2008) or a combination with apparent oxygen utilization (AOU) and seawater age identified by the isotope (e.g., ^{3}H and ^{3}He) (Feely et al. 2004; Xie et al. 2021).

Despite the importance of constraining TZR, the current estimates based on the different approaches appear hard to reconcile, and the discrepancy sometimes can reach an order of magnitude within the same basin (Steinberg et al. 2008; Martínez-García 2016). For example, the TZR measured by *in vivo* INT approach (13.2 mol C m^{-2} yr^{-1}) in the North Pacific subtropical gyre (station ALOHA) is over 7 times higher than that determined by the PR + ZR approach (synthesis of prokaryotic respiration determined by radiolabeled leucine incorporation and zooplankton respiration empirically estimated from the biomass) (1.5 mol C m^{-2} yr^{-1}) (Steinberg et al. 2008; Martínez-García 2016). Similarly in North Atlantic Subtropical Gyre, a recent study by Arístegui et al. (2020) based on *in vitro* INT reported a much higher TZR (28.4 mol C m^{-2} yr^{-1}) than the previous estimate from the net oxygen utilization rate (4.5 mol C m^{-2} yr^{-1}) (Jenkins 1982). It remains unclear if this discrepancy is associated with the biases in a specific approach or reflects different spatiotemporal scales of TZR captured by different approaches. Furthermore, these diverging TZR estimates pose a significant challenge in understanding the balance between the carbon demand at depth and carbon supply from the upper layer (Steinberg et al. 2008; Fernández-Urruzola et al. 2021). Over the past two decades, increasing evidence has implied that sinking particle flux is not the only carbon source that contributes to carbon remineralization at depth. Other processes, such as the downward mixing of dissolved organic carbon (DOC) (Arístegui et al. 2002; Emerson 2014), dark carbon fixation (DCF) by chemoautotrophs (Shen et al. 2020; Saxena et al. 2022), lateral transport of organic matter (Shen et al. 2020; Kelly et al. 2021), and active transport by the diel vertical migrators (Giering et al. 2014; Archibald et al. 2019), can also act as significant carbon sources to fuel the TZR. To date, only a few studies (e.g., the Porcupine Abyssal Plain site in the north Atlantic) have succeeded in balancing the carbon demand by incorporating multiple carbon supply sources (Giering et al. 2014). It requires further vetting to assess whether such a framework can be achieved in other regions.

The South China Sea (SCS) is the largest marginal sea of the western Pacific Ocean, influenced by Asian monsoons (Chen et al. 2001). Despite being oligotrophic, the central SCS basin experiences active water mass and organic matter exchange with the adjacent continental shelf and western Pacific, resulting in unique biogeochemistry (Wu et al. 2015; Shen et al. 2020; Dai et al. 2022). The upper layer carbon export in the SCS has been estimated by various approaches such as sediment traps (Lahajnar et al. 2007; Ran et al. 2015; Shen et al. 2020), ^{234}Th-^{238}U disequilibrium (Cai et al. 2008; Zhou et al. 2013; Cai et al. 2015), nitrate-based new production (Chen, 2005), satellite-based model (Li et al. 2018) and mass balance of oxygen (Huang et al. 2018), falling in a range of 0.8–3.1 mol C m^{-2} yr^{-1}. In contrast, TZR remains poorly constrained, with only limited studies on prokaryotic production and oxygen utilization rates (Shen et al. 2020; Xie et al. 2021). In this study, we applied three independent approaches, including BGC-float observation, *in vivo* INT and PR + ZR, to quantify the TZR in the SCS basin. Piecing together with an integrated analysis of multiple carbon supply sources from the literature, we aim to address the following questions:

1. What is the magnitude of TZR in the SCS basin and which methods are more reliable?
2. Can the carbon demand in the twilight zone be balanced with comprehensive carbon supply sources?

2. Methods

2.1. Study region

Our study region (11.0°N–21.7°N, 110°E–118.5°E) is located in the central SCS basin (Fig. 1), a typical oligotrophic area characterized by low chlorophyll *a* and depleted nutrients in the surface (Chen et al. 2001; Ning et al. 2004; Zhang et al. 2016). The meteorological forcing in this region is dominated by the East Asian Monsoon with the northeast monsoon prevailing from November through April (cold season), and the southwest monsoon between June and September (warm season) (Liu et al. 2002; Dai et al. 2022). The monthly climatology euphotic zone, derived from the Moderate Resolution Imaging Spectroradiometer (MODIS) (https://oceandata.sci.gsfc.nasa.gov) in the SCS basin is relativity constant over the year (~98 m) (Fig. S1). For simplicity, we set 100 m as an upper boundary of the twilight zone.

2.2. Multiple approaches for estimating the TZR

2.2.1. Oxygen mass balance model based on BGC-float observation

The floats data used in this study were from two Sea-Bird Scientific Navis floats (numbered F0347 and F0348), and one PROVOR NKE float (numbered XMU-001b) deployed by Xiamen University, China (yellow line in Fig. 1a). These floats were conducted profiling cycles every 1–5 days with a vertical resolution of 2 m from surface to 1000 m depth and 50 m below 1000 m depth. Over 700 profiles were collected by three floats from July 2014 to July 2019. The raw O_2 data were calibrated using the simultaneous shipboard oxygen samples measured by the high-precision Winkler titration during floats deployment (Fig. S2). The float-measured temperature, salinity, and oxygen were interpolated linearly into 1 m depth resolution and then smoothed over time using a five-point running-mean filter to remove the short-term fluctuation (Huang et al. 2022).

We constructed a simplified 1-D twilight zone oxygen mass balance model (Eq. (1), Fig. S3) by neglecting the lateral transport following Hennon et al. (2016) and Billheimer et al. (2021):

$$\frac{\partial O_2}{\partial t} = F_{Bio} + F_{\kappa z_{net}} \quad (1)$$

where $\frac{\partial O_2}{\partial t}$ is the float observed O_2 change in the seawater, F_{Bio} is

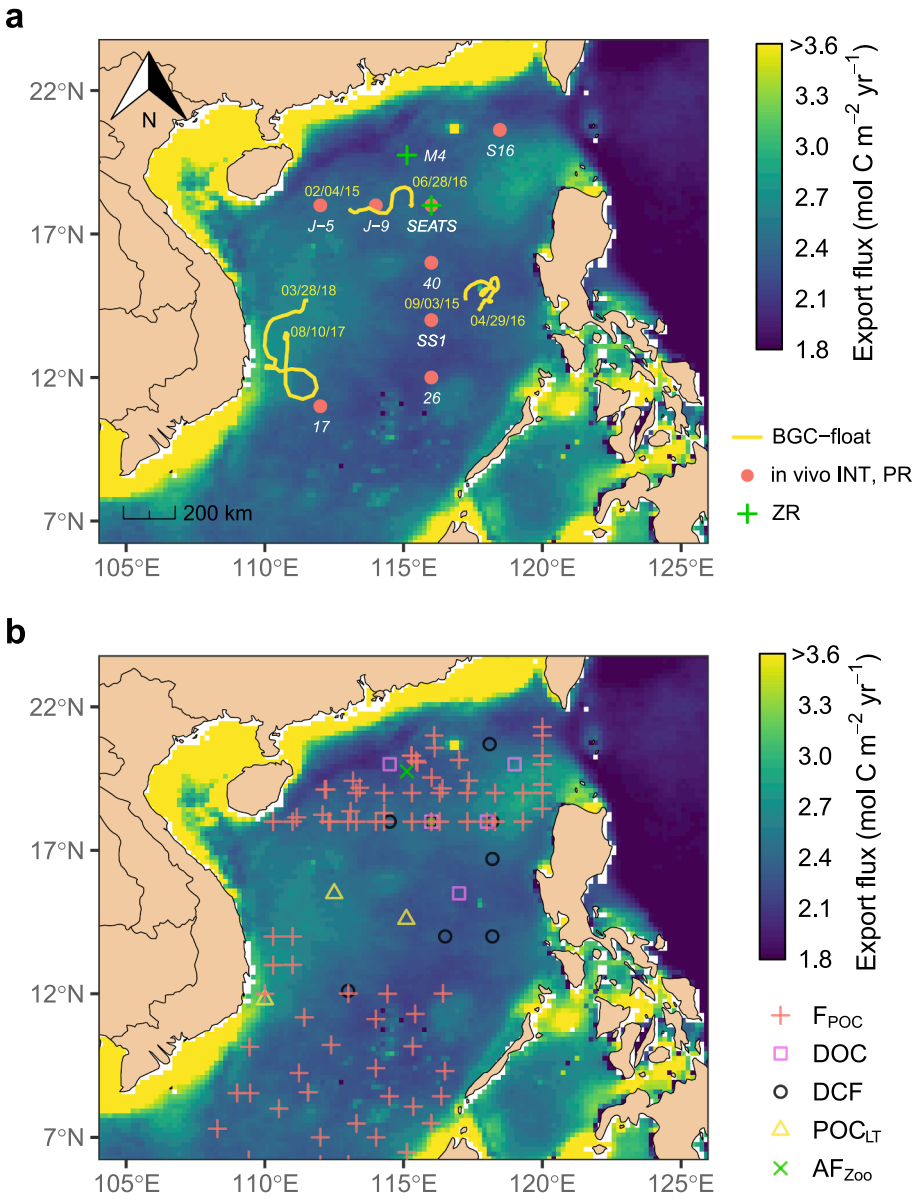

Fig. 1. Study region in the South China Sea (SCS) basin. (a) sampling sites of the twilight zone remineralization; (b) the compiled dataset of multiple carbon supply sources from historical studies. The yellow numbers in panel a represent the sample period of the BGC-float used in this study (mm/dd/yy). The background color shows the climatology of annual export production from the satellite estimate (Supplementary Methods). BGC-float: biogeochemical profiling floats; *in vivo* INT: the reduction of tetrazolium salt by the cellular electron transport system; PR: prokaryotic respiration; ZR: zooplankton respiration; F_{POC}: particulate organic carbon sinking flux; DOC: dissolved organic carbon; DCF: dark carbon fixation; POC_{LT}: lateral transport of POC; AF_{Zoo}: active flux by zooplankton diel vertical migration.

biological oxygen consumption, $F_{\kappa z_{net}}$ is net diapycnal eddy diffusion, resulting from the difference of fluxes between the top and bottom boundaries at each isopycnal layer (Eq. (2)).

$$F_{\kappa z_{net}} = F_{\kappa z_{top}} - F_{\kappa z_{bottom}} = K_{z_{top}} \times \frac{\partial O_2}{\partial z}_{top} - \kappa_{z bottom} \times \frac{\partial O_2}{\partial z}_{bottom} \quad (2)$$

$\frac{\partial O_2}{\partial z}$ and κ_z represent vertical oxygen gradient, and diapycnal diffusivity coefficient, respectively. The oxygen mass balance model was implemented alongside the isopycnal surface (σ_θ) to eliminate the oxygen change induced by the vertical displacement (Billheimer et al. 2021; Wang and Fennel 2022). The density intervals were set to 0.35 kg m^{-3} when $\sigma_\theta \leq 26.0$ kg m^{-3} and 0.1 kg m^{-3} when $\sigma_\theta > 26.0$ kg m^{-3} (Fig. S4). $\frac{\partial O_2}{\partial t}$ was computed as a slope (fitted by the least squares linear regression) of the seasonal oxygen evolution (Hennon et al. 2016; Wang and Fennel 2022). κ_z was set to 10^{-5} m^2 s^{-1}, following the values reported by Shang et al. (2017) and He et al. (2022), which were directly measured using the Turbulence Ocean Microstructure Acquisition Profiler in our study region.

In most of the time, the deployed floats were parked at a depth of 1000 m and can generally be considered as quasi-Lagrangian drifters that follow the same water mass (Lacour et al., 2019). Therefore, the oxygen changes observed by the floats is less affected by the horizontal advection. To further minimize this error, we visually inspected the float data and discarded the periods that experiencing the notable fluctuation in spice anomalies (Klymak et al. 2015; Long et al. 2016) (Fig. S4d–4f). Finally, 30 profiles (from February 4, 2016 to June 28, 2016, spanning 145 days) from F0347, 67 profiles (from September 3, 2015 to April 29, 2016, spanning 239 days) from F0348, and 44 profiles (from August 10, 2017 to March 28, 2018, spanning 230 days) from XMU-001b were retained for F_{Bio} calculation (Fig. 1a, Fig. S4g–4i). To facilitate the comparison, the oxygen-based respiration was converted into the carbon unit using the respiration quotient ($RQ_{O_2:C}$) of 1.45 (Anderson and

Sarmiento 1994).

2.2.2. *In vivo* INT

The reduction rate of the tetrazolium salt 2-(p-iodophenyl)-3-(p-nitrophenyl)-5-phenyltetrazolium chloride (INT) to INT formazan (INT_F) by electron transport system dehydrogenase enzymes can be indicative of planktonic respiration. This method has become increasingly popular for measuring respiration in the oligotrophic ocean and twilight zone because of its high sensitivity and precision (Martínez-García et al., 2009; García-Martín et al. 2019). Samples for measuring the INT reduction were collected aboard the R/V *Tan Kah Kee* from two cruises (KK2004 cruise: 30 August 2020 to 30 September 2020; KK2102 cruise: 27 July 2021 to 30 August 2021; the red dot in Fig. 1a) using Niskin bottles attached to a Sea-Bird conductivity-temperature-depth (CTD) rosette sampler at eight depths (100, 150, 200, 300, 400, 600, 800, 1000 m).

We adopted a modified approach described by Martínez-García et al. (2009) to measure *in vivo* INT reduction rates. We performed time-course experiments to determine the optimum incubation time, which was four hours, to ensure a linear increase of reduced INT within the incubation period and to avoid the toxicity of INT and INT_F to the living cells (Fig. S5). At each depth, we set up four replicates (incubation volume: 500 mL), one of which was immediately killed by adding formaldehyde (2% w/v final concentration) as a control. Fifteen minutes later, all replicates were inoculated with a sterile solution of INT (0.2 mmol L^{-1} final concentration, Sigma, USA) and incubated in temperature-controlled (*in situ* temperatures, ±1 °C) chambers for four hours. After incubation, samples were fixed by adding formaldehyde (2% w/v final concentration) and filtered through 47 mm diameter 0.2 μm pore size polycarbonate membrane filters (Millipore, USA). After a 15-minute stand, the reduced INT (formazan, INT_F) retained on each filter membrane was extracted and stored frozen in 2 mL cryovials at −20 °C until further processing. Back in the lab, the INT_F was extracted from the filters using propanol, and its concentration was determined by a microplate reader (Perkin Elmer, USA). We used the empirical ratio of 12.8 mol O_2 mol INT_F^{-1} suggested by Martínez-García et al. (2009) to convert the reduction rate of INT into the oxygen consumption rate.

2.2.3. *Synthesis of prokaryotic and zooplankton respiration (PR + ZR)*

TZR can be computed as a sum of respiration attributed by the prokaryote and zooplankton, following Giering et al. (2014). PR was estimated from the prokaryotic production measured by radioactive leucine (^{3}H-leucine) uptake, in the combination with the prokaryotic growth efficiency (Smith and Azam 1992). The PR samples were collected from eight depths, consistent with the sampling depth of *in vivo* INT approach. For each depth, triplicate samples (3.6 mL unfiltered seawater in a 5 mL centrifuge tube) and one replicate blank (fixed with 200 μL of 100% trichloroacetic acid, TCA) were inoculated with ^{3}H-leucine (specific activity of 40–60 Ci mmol L^{-1}, Perkin Elmer, USA; final concentration of 10 nmol L^{-1}) and incubated in the dark at *in situ* temperatures (±1 °C) for 4 h. After incubation, samples and blanks were all fixed with 200 μL of 100% TCA to terminate the reaction and then were kept at −20 °C until further processing. The thawed samples were filtered by 0.2 μm polycarbonate membranes (25 mm diameter, Millipore, USA), and the centrifuge tubes were washed sequentially with ice-cold 5% TCA and 80% ethanol 2–3 times. The filters were placed in 3.5 mL scintillation cocktail (Perkin Elmer, USA) and stood for 48 h. The radioactivity incorporated into cells was counted in a liquid scintillation counter (Tri-Carb 2800TR, Perkin Elmer, USA). The leucine incorporation rates were calculated by differencing the mean disintegrations between the control and incubation samples. PR was estimated using the following equation (Eq. (3)),

$$PR = leucineincorporation \times LeuCF \times \frac{(1 - PGE)}{PGE} \quad (3)$$

where the LeuCF is the leucine-carbon conversion factor, and PGE is the prokaryotic growth efficiency. In the global ocean, LeuCF and PGE have been reported to exhibit a significant spatial variability, which is closely linked to the availability of nutrients and organic carbon in the seawater (del Giorgio and Cole, 1998; Giering et al., 2014; Smith et al., 2021). To ensure the accuracy of our regional estimates, we conducted a comprehensive review of the existing literature to determine the appropriate values for our study. For LeuCF, we adopted a value of 0.41 ± 0.09 kg C mol^{-1} leu, which is derived from local incubation experiments conducted in previous study (Shen et al. 2020). This regional value is closely aligned with the median LeuCF of 0.54 for the global mesopelagic zone reported by a recent synthesis study by Giering and Evans (2022). Due to the lack of direct measurements of PGE in our study site, we compiled historical data on PGE from the twilight zone across the global ocean and used the global median PGE of 0.07 in our study (Fig. S6). We further use the global PGE interquartile range of 0.03–0.09 to simulate the uncertainty (Table S2). Additionally, to evaluate the sensitivity of our PR estimation to LeuCF and PGE, we reconstruct PR with 1281 combinations of LeuCF (range from 0.30 to 0.50 with increments of 0.01) and PGE (range from 0.03 to 0.09 with increments of 0.001) (Fig. S7).

Zooplankton samples were collected aboard the R/V *Tan Kah Kee* from 19 June 2019 to 26 June 2019 (KK1906 cruise) at stations M4 and SEATS using MultiNet (0.25 m^2, 200-μm mesh, HYDRO-BIOS, Germany) (green cross in Fig. 1a). At each station, we carried out repeated vertical, high-resolution net tows at five depth horizons (0–50 m, 50–100 m, 100–200 m, 200–400 m, 400–700 m) during both day and night (four times at station M4 and six times at station SEATS, the daytime is defined as the period between 6:00 and 18:00). Samples were split into two parts: half for biomass and elemental analysis, and the other half for taxon and abundance analysis. ZR (μg C m^{-3} h^{-1}) was empirically estimated from samples as a function of zooplankton nitrogen weight (NW, mg m^{-3}) and seawater temperature (T, °C), following Al-Mutairi and Landry (2001):

$$ZR = exp(1.74 + 0.85 \times ln(NW) + 0.064 \times T) \times \frac{1}{RQ_{O_2:C}} \times \frac{12}{22.4} \quad (4)$$

where $RQ_{O_2:C} = 1.45$ is the respiratory quotient and 12/22.4 is the molar conversion factor (Anderson and Sarmiento, 1994). The NW and T were measured by the elemental analyzer (2400 CHN Analyzer, Perkin Elmer, USA) and CTD sensor, respectively. To obtain ZR profiles matching the depths of PR, we extrapolated the ZR observation by using a power law function (Fig. S8). Subsequently, we combined these two mean profiles to generate an overall mean profile for bulk respiration (PR + ZR) in the SCS. It's worth noting that the magnitude of ZR is approximately only 10% of that of PR, as indicated in Fig. S9. Consequently, the bulk respiration estimate obtained through this method is predominantly influenced by the PR values. Therefore, the spatial mismatch between the sampling stations for ZR and PR has a relatively limited impact on the final bulk respiration estimate.

2.3. *Compilation of potential carbon supply*

To constrain the possible range of TZR and reconcile the regional carbon budget in the SCS basin, we synthesized and reanalyzed a variety of possible carbon sources from the literature following the framework proposed by Giering et al. (2014). These sources include upper particulate organic carbon (POC) sinking flux, DOC input, active carbon transport via zooplankton diel vertical migration, DCF by chemoautotrophs, and lateral transport of POC. For each carbon source, we computed the ensemble mean and standard deviation (as an uncertainty) of the compiled dataset.

2.3.1. *POC sinking flux, DCF, and lateral transport of POC*

Upper layer ^{234}Th-based POC sinking flux was compiled from a set of

historical studies (Cai et al. 2008; Zhou et al. 2013; Cai et al. 2015). The pooled dataset consists of 72 stations sampled in four seasons, providing good spatial coverage of the SCS basin (Fig. 1b). DCF in the twilight zone was derived from snapshot measurements in 8 stations (Fig. 1b) compiled from prior studies by Shen et al. (2020), which was determined by radioactive ^{14}C incorporation rates.

The amount of lateral transport POC originating from the northern, productive shelf has been indirectly estimated in the prior study by Shen et al. (2020). The authors compared the difference in POC sinking flux between theoretical and *in situ* observation from moored sediment traps. The theoretical POC sinking flux at various horizons was inferred from the POC flux at the base of the euphotic zone using the Martin Curve applying an attenuation coefficient b of 0.95 (a value derived from the location in the absence of lateral transport influence, see details in section 2 in Shen et al. 2020). Given that no significant lateral transport was found in the southern SCS basin (Shen et al. 2020), we set the lateral transport of POC to 1.1 ± 0.2 mol C m^{-2} yr^{-1} (half of the lateral transport of POC obtained in the northern SCS) to approximate the average shelf-to-basin transport of POC in the entire SCS basin.

2.3.2. DOC supply

The fraction of TZR fueled by the DOC portion (TZR_{DOC}) can be calculated as follows (Arístegui et al. 2002; Emerson 2014; Giering et al. 2014)

$$TZR_{DOC} = \int_{100\ m}^{1000\ m} TZR\ dz \times RQ_{O_2:C} \times \frac{DOC}{AOU} \quad (5)$$

where $\frac{DOC}{AOU}$ is the slope of the linear regression between DOC and AOU derived from three historical cruises (including 6 sampling stations during summer, fall, and winter seasons, Fig. 1b, Table S1) (Hung et al. 2007), and $\int_{100\ m}^{1000\ m} TZR\,dz$ is the depth-integrated respiration rate (here we used average TZR determined by BGC-float and PR + ZR given they provide more reasonable constraints, see Discussion section).

2.3.3. Active carbon transport by zooplankton diel vertical migration

Another source of DOC is the active flux by zooplankton diel vertical migration. The active flux may be not included in the calculation of the DOC-AOU method mentioned above because it is often regarded as an episodic event and thus calculated separately (Emerson 2014; Giering et al. 2014). Active carbon transport was estimated by assuming that DOC excretion by migrating zooplankton is roughly equivalent to 31% of their respiration (Steinberg et al. 2000; Giering et al. 2014). The fraction of zooplankton associated with migration was distinguished by comparing the difference between samples collected during the day and night (Fig. S10). We excluded carbon transport induced by defecation and mortality due to the large uncertainties in their estimation (Giering et al. 2014).

2.4. Uncertainty estimates and statistical analysis

Propagated error for each TZR method consists of spatial variability (σ_v) among the sampling stations (calculated as a standard error) and the aggerated error (σ_a) inherited from a range of sources such as the instrument (e.g., oxygen sensor), and parameterization (e.g., uncertainty in diapycnal κ_z, LeuCF, and PGE, etc.). The σ_a was quantified using the Monte Carlo approach interaction with the magnitude of error assignment presented in Table S2. The propagated error was calculated as $\sqrt{\sigma_v{}^2 + \sigma_a{}^2}$. Power law functions were selected to fit the discrete TZR measurement, as they better described the remineralization profiles (Table S3). The mean and standard error of the scaling exponent b was estimated through log–log linear regression on the log-transformed data, which is the standard approach for fitting power law models. The significance was satisfied if the p-value < 0.05. Data analysis and visualization were performed using R 4.1.2 (R Core Team 2021).

2.5. Caveats and limitations

In our study, we considered the SCS basin as a whole and linked TZR and multiple carbon supply pathways collected from various stations and sampling periods. This analysis might be somewhat confounded by the spatiotemporal mismatches and uncertainty inherited from each methodology. For example, TZR estimated from BGC-float observation is based on the oxygen drawdown over the seasonal scale, whereas *in vivo* INT and PR + ZR were snapshot measurements during the summer and autumn. Nonetheless, the twilight zone is generally characterized by weak seasonality (Fig. S11), as the seasonal forcing gradually diminishes with increasing depth. Despite our sampling efforts spanning different seasons and locations, the coefficients of variation (CV = standard deviation/mean × 100%) of respiration rates determined by BGC-float, *in vivo* INT, PR and ZR are 25.8%, 30.0%, 48.6% and 29.8%, respectively (Fig. 2). The low CVs indicate a relatively spatial and temporal homogeneity in the twilight zone of the central basin. The large-scale upper layer net primary production and carbon export (background color in Fig. 1 and Fig. S13) predicted by the remotely sensed algorithm also reveals a relatively spatiotemporal uniform in the sunlit ocean within the central basin, supporting the rationale to treat the South China Sea central basin as an entirely for an integrated analysis. Moreover, we found that methodological discrepancies for TZR measurements, the focus of our study, are the primary factor causing the observed difference in the TZR, rather than spatiotemporal mismatches (see Results and Discussion section).

Our compiled dataset of POC sinking flux covers four seasons, generally providing a representative annual flux (Fig. 1b, Fig. S12). For other carbon supply terms, such as DCF, lateral transport, DOC input and active transport flux, the compiled dataset only one or two seasons. Despite these caveats, it should be noted that to date, only a few field studies have achieved co-located, simultaneous measurements of these complex processes (Giering et al., 2014). Our study provides a feasible basin-scale example and demonstrates how field observations and historical measurements can be leveraged to advance our understanding of the TZR and regional carbon budget. The methodological discrepancy and critical carbon supply pathways to sustain the regional carbon budget identified from our analysis can also help guide future fieldwork.

3. Results

3.1. Comparison of TZR among three approaches

TZR depth profile determined from three approaches generally exhibited exponential decay over depth (Fig. 2, Fig. 3a), with 80% remineralization occurring in the upper 400 m (Fig. 3b, c). Albeit there are some subtle differences in the respiration profiles among the three methods, the power-law fitting curves based on normalized TZR show high degree of consistency (Fig. 3b). The attenuation coefficients (b value) of TZR were found to be the same within the uncertainty for all three approaches, with the respective value of 1.00 ± 0.11 (mean ± SE) for BGC-float observation, 0.87 ± 0.10 for *in vivo* INT, and 0.90 ± 0.13 and for PR + ZR (Fig. 3b, Table S3).

The volumetric TZR determined from the seasonal oxygen drawdown via the BGC-float observations, ranged between 0.002 mmol C m^{-3} d^{-1} and 0.06 mmol C m^{-3} d^{-1} (Fig. 2a). In contrast, volumetric rates measured by *in vivo* INT approach was approximately one order magnitude higher than the BGC-float estimates, displaying exponential decrease from a maximum of 0.6 mmol C m^{-3} d^{-1} at the base of euphotic zone to a minimum of 0.0003 mmol C m^{-3} d^{-1} around depths of 800–1000 m (Fig. 2b). Our third approach to calculate bulk respiration involves summing the contributions of respiration by prokaryotes and zooplankton, with prokaryotes being the predominant contributors to bulk respiration (as illustrated in Fig. 2c and 2d). Overall, the volumetric rates of PR fall within a similar range as the TZR obtained from BGC-float measurements. ZR, on the other hand, constitutes less than 10%

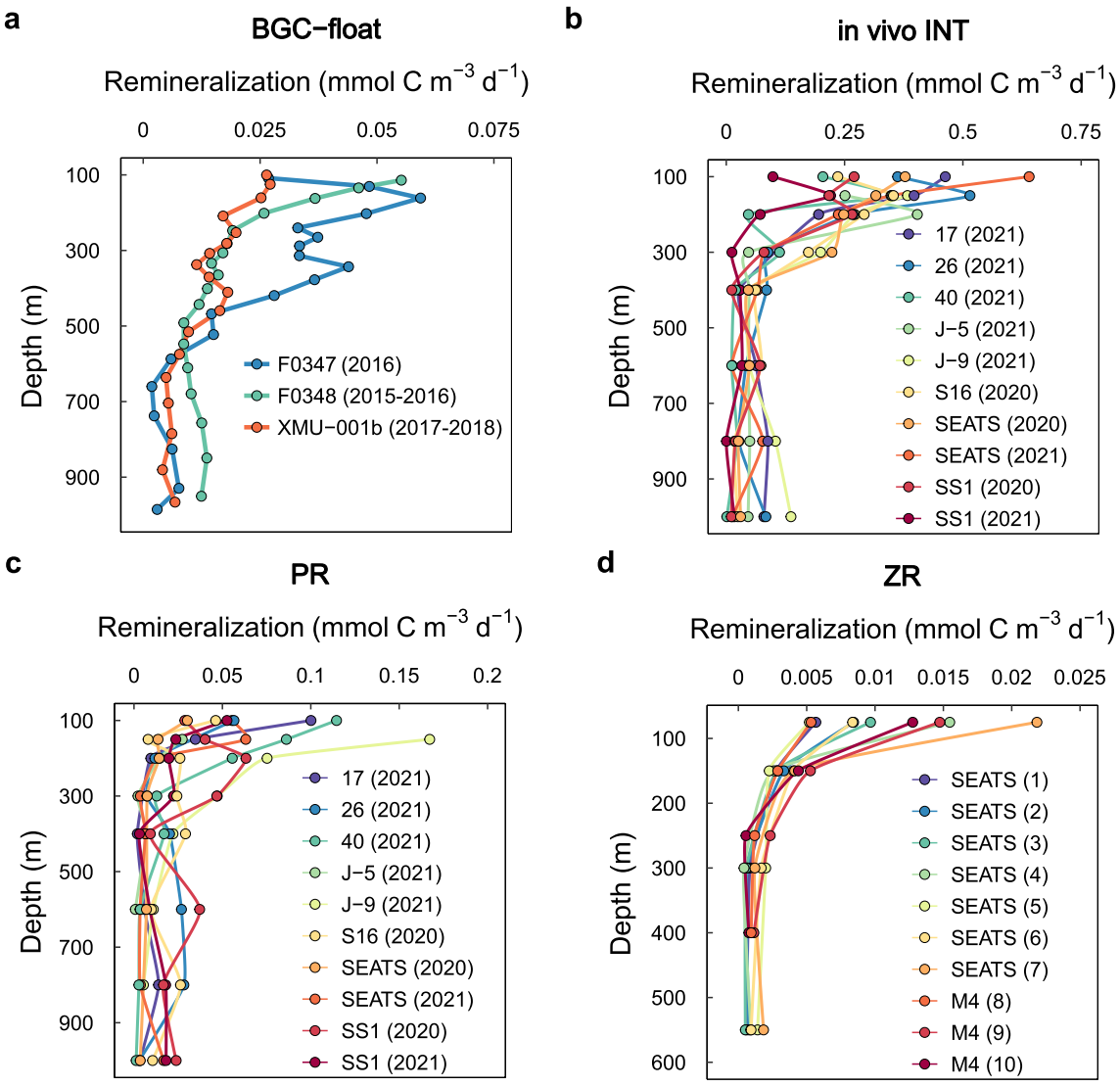

Fig. 2. Depth-resolved profiles of bulk respiration measured by **(a)** biogeochemical profiling floats (BGC-float), **(b)** the reduction of a tetrazolium salt by the cellular electron transport system (*in vivo* INT), **(c)** prokaryotic respiration determined by radiolabeled leucine incorporation (PR), and **(d)** zooplankton respiration empirically estimated from the biomass (ZR). The numbers in parentheses in panels a, b, and c represent years of sampling. The numbers in parentheses in panel d represent times of zooplankton net tows.

of bulk respiration and varies between 0.0003 mmol C m^{-3} d^{-1} and 0.03 mmol C m^{-3} d^{-1}. The depth-integrated TZR between 100 m and 1000 m determined by BGC-float (5.1 ± 0.5 mol C m^{-2} yr^{-1}) was also close to that of PR + ZR (6.4 ± 3.0 mol C m^{-2} yr^{-1}); while depth-integrated TZR determined by *in vivo* INT (30.0 ± 6.1 mol C m^{-2} yr^{-1}) was one order of magnitude higher than the counterparts determined by the other two approaches (Fig. 3d).

3.2. Carbon supply from multiple sources

Overall, the total carbon supply to the twilight zone estimated from our compiled dataset was 4.8 ± 1.3 mol C m^{-2} yr^{-1} (Fig. 4, Table 1), which is close to the TZR determined by BGC-float observation (5.1 ± 0.5 mol C m^{-2} yr^{-1}) and PR + ZR (6.4 ± 3.0 mol C m^{-2} yr^{-1}) within the uncertainty. Among carbon sources, POC flux export from the base of the euphotic zone accounts for ~40% of the total carbon supply, with an estimated value of 1.9 ± 1.2 mol C m^{-2} yr^{-1}. The amount of TZR sustained by the DOC portion and POC input through lateral transport contributed nearly equally, yielding values of 1.1 ± 0.4 mol C m^{-2} yr^{-1} and 1.1 ± 0.2 mol C m^{-2} yr^{-1}, respectively. The ammonia-oxidizing archaea and nitrite-oxidizing bacteria-mediated DCF supply 14.6% of the total organic carbon sources (0.7 ± 0.4 mol C m^{-2} yr^{-1}). By contrast, the active flux via the zooplankton diel vertical migration contributes minimally to the total carbon supply (0.01 ± 0.02 mol C m^{-2} yr^{-1}) (Fig. 4, Fig. S10).

4. Discussion

To our knowledge, this is the first study to apply three independent approaches to constrain the TZR in the same ocean basin. By further combining with the integrated analysis of multiple carbon supply sources, we provide more insight into the potential methodological discrepancy in TZR measurements. In the following sections, we first compared our TZR estimates to those from the global ocean and then discussed possible reasons for the observed differences in TZR among the three approaches. Finally, we analyzed the regional carbon budget in the SCS basin by examining the balance between carbon supply and demand.

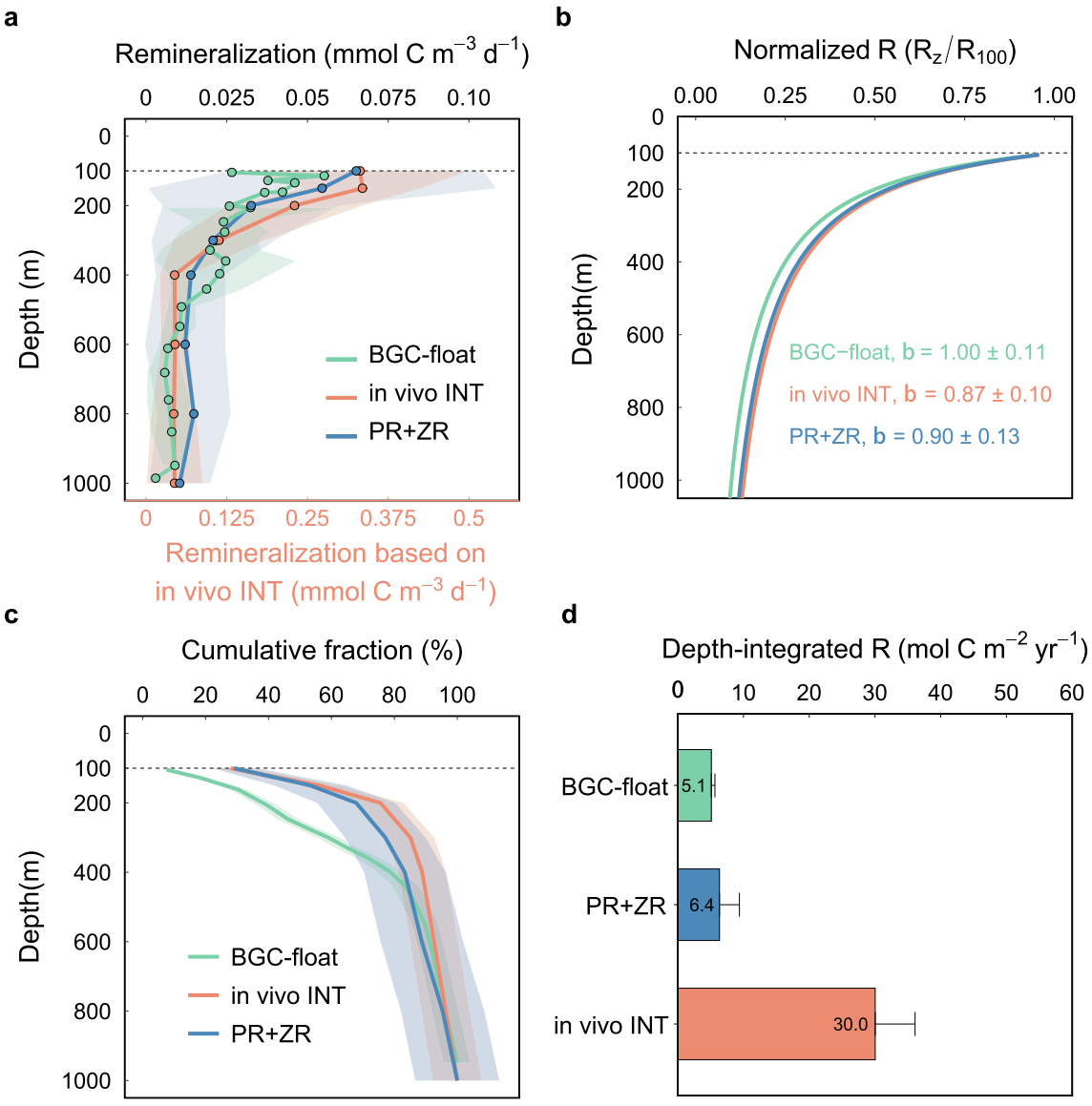

Fig. 3. Twilight zone remineralization (TZR) determined by three approaches in the South China Sea basin. (**a**) Depth profiles; (**b**) the fits of power law function of TZR normalized to the base of the euphotic zone (100 m); (**c**) depth-cumulative fraction; (**d**) depth integration. The horizontal dashed line in panels a-c indicates the euphotic zone depth. The annual depth-integrated TZR in panel d is computed by integrating daily TZR in shown panel a, and then multiplying the results by the day length of each year (365 days) assuming a steady flux throughout the year. The shading in panels a and c, and the horizontal bar in panel d represent the propagated error. BGC-float: biogeochemical profiling floats; *in vivo* INT: the reduction of a tetrazolium salt by the cellular electron transport system; PR + ZR: synthesis of prokaryotic respiration and zooplankton respiration; b: attenuation coefficient of TZR fitted by the power law function.

4.1. Comparison of TZR estimate in the SCS basin with the global ocean

Vertical profiles of TZR measured by three approaches cohesively decline exponentially with depth (Fig. 2, 3), which is well-fitted by the power law function. The average TZR attenuation coefficient is around 0.87–1.0, comparable with the prior studies of 0.56–0.94 in Terrace Bay (20.2°S–20.3°S, 8.0°E–12.3°E, *in vitro* INT approach) (Osma et al. 2014) and 0.87–1.22 off the northern Chilean coast (20.1°S–24.0°S, 70.0°W–72.5°W, *in vitro* INT approach) (Fernández-Urruzola et al. 2021).

TZR measured by PR + ZR in the SCS basin was 6.4 ± 3.0 mol C m^{-2} yr^{-1}, ~23% higher than the upper bound of the estimates in other regions (1.8–5.2 mol C m^{-2} yr^{-1}, Table 2) determined by the same approach. But this finding aligns with high prokaryotic respiration (5.6 mol C m^{-2} yr^{-1}) reported by Shen et al. (2020) in the SCS basin, which accounts for over 90% of total TZR (Fig. 2, Fig. S9). Similarly, the TZR derived from the seasonal oxygen drawdown based on BGC-float observation (5.1 ± 0.5 mol C m^{-2} yr^{-1}), is also at the high end of the range (2.0–5.1 mol C m^{-2} yr^{-1}) of oxygen utilization rate in the subtropical oceans (Table 2), but comparable to those in the subpolar North Atlantic (4.5 mol C m^{-2} yr^{-1}) and subantarctic Southern Ocean (4.4 ± 2.9 mol C m^{-2} yr^{-1}). Using the isotope of ^{3}H and ^{3}He to track the seawater age, Xie et al. (2021) obtained a relatively low subsurface apparent oxygen utilization rate (1.96 ± 0.2 mol C m^{-2} yr^{-1}) in the SCS basin. This discrepancy might be partly attributed to the different time scales of TZR captured by the two approaches. The isotopes-based approach tends to reflect the oxygen consumption rate corresponding to the residence time of ^{3}H (typically 3–50 years, depending on the depth) (Xie et al. 2021), providing a measure close to a steady state. By contrast, our float estimate based on the seasonal oxygen drawdown reflects a more instantaneous signal that integrates the impact inherited from episodic carbon supply events (Hennon et al. 2016; Billheimer et al. 2021). Similarly, Koeve and Kähler (2016) recently reported that the AOU-over-age approach may lead to an underestimation of the

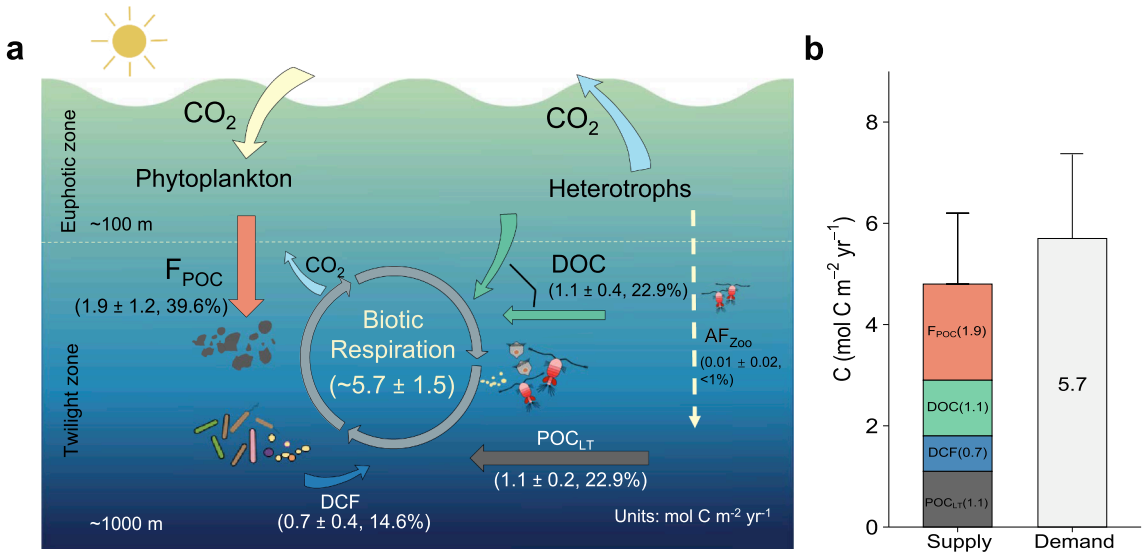

Fig. 4. **(a)** Schematic diagram illustrating the different processes contributing to the regional carbon budget, and **(b)** synthesis of estimated carbon supply and demand in the South China Sea basin. Carbon demand is estimated from the average remineralization rates in the twilight zone determined by biogeochemical profiling floats and the synthesis of prokaryotic respiration and zooplankton respiration. The percentage in the parentheses in panel a denote the fractional contribution of each process to the total carbon supply. The active carbon transport by the zooplankton migration (AF_{zoo}) is not included in panel b due to its minimal contribution. The bar in panel b represents propagated uncertainty. F_{POC}: upper layer sinking flux of particulate organic carbon; DOC: dissolved organic carbon input; DCF: dark carbon fixation by chemoautotrophs; POC_{LT}: lateral transport of particulate organic carbon.

respiration by a factor of 3 due to the nonproportional diffusive mixing of AOU and water age (i.e., the proportions of AOU and water age changed by advection and mixing processes).

TZR measured by the INT reduction approach in the global ocean varies widely, ranging from 3.8 mol C m^{-2} yr^{-1} to 28.2 mol C m^{-2} yr^{-1} (Table 2). In our study region, *in vivo* INT reduction approach yields a value of 30.0 ± 6.1 mol C m^{-2} yr^{-1} (Fig. 3d), approximating the maxima historical estimate in the subtropical North Atlantic (28.2 ± 4.9 mol C m^{-2} yr^{-1}) (Arístegui et al. 2020). Yet, it is important to note that the compiled dataset of INT-based TZR estimates differs in techniques used to derive the INT reduction rate: *in vivo* INT and *in vitro* INT (depending on the respiration measurement whether in the living cell, see more details in Martínez-García et al., 2009). In principle, *in vivo* approach is thought to provide a more realistic estimate of TZR whereas *in vitro* INT tends to reflect the maximum potential respiration rates (Martínez-García et al., 2009). Nevertheless, no systematic difference is observed between the two approaches, probably due to the limited number of data points (Table 2). Overall, three independent approaches applied in our study, despite the existing methodological discrepancy, seem to imply a relatively high TZR in the SCS basin, for possible mechanisms we will discuss in the following sections.

4.2. The discrepancy among the three approaches

In general, BGC-float observation (5.1 ± 0.5 mol C m^{-2} yr^{-1}) and PR + ZR (6.4 ± 3.0 mol C m^{-2} yr^{-1}) show a more consistent estimate of TZR in the SCS basin, yielding values that can balance the amount of known carbon supply within the uncertainty bounds (Fig. 4, 5.7 ± 1.5 mol C m^{-2} yr^{-1}). By contrast, *in vivo* INT approach gave rise to an extremely high TZR, reaching up to 30.0 ± 6.1 mol C m^{-2} yr^{-1}. Similar paradoxes were also identified at the North Pacific subtropical gyre (station ALOHA) and North Atlantic subtropical gyre, in which the INT reduction approach gave rise to a value 6–7 times higher than the counterpart estimated by the other two approaches (Table 2). Despite this difference, the vertical pattern of TZR determined by *in vivo* INT collaborates well with the other two approaches (Fig. 2b, 3b), suggesting *in vivo* INT is capable of accurately capturing the vertical attenuation of TZR but might misrepresent results in the terms of magnitude.

In our study, we applied a scaling factor of 12.8 mol O_2 mol INT_F^{-1} to convert the INT reduction rate into oxygen consumption (Table 2), which is recommended by the original methodology article of Martínez-García et al. (2009) and subsequently adopted by another study in the twilight zone of North Pacific subtropical gyre (Martínez-García 2016) (Table 2). Recently, García-Martín et al. (2019) proposed a new linear relationship based on the global dataset of paired measurements of *in vivo* INT and direct oxygen consumption rates derived from the 24-hour bottle incubation in the upper ocean (<200 m). However, applying this empirical equation results in a higher TZR in our study region (52.2 ± 8.7 mol C m^{-2} yr^{-1}). Some studies have shown evidence that the oxygen consumption rate from bottle incubation might be considerably overestimated as a result of the artificial stimulation of bacterial growth and enhanced DOC cycling in the enclosed space (Martínez-García et al., 2009; Huang et al. 2019a). As such, the conversion factor (12.8 mol O_2 mol INT_F^{-1}) scaled from the bottle incubation-based oxygen consumption rate might be overestimated. Additionally, INT reduction is not cell-specific for the respiration system and sensitive to many substances such as ascorbic acid, cysteine, and glutathione, depending on the microbial community (Maldonado et al. 2012). It's worth noting that previously reported scaling factors for INT reduction have been derived from either laboratory cultures containing a single eukaryotic species (e.g., *Isochrysis galbana*, Martínez-García et al., 2009) or seawater samples from the upper layer, which consist of a mixture of eukaryotic and prokaryotic organisms (Martínez-García, 2016). In contrast, the microbial community in the twilight zone is predominantly composed of prokaryotic groups. Additionally, a recent study conducted by Baños et al. (2020) has raised concerns regarding the potential toxicity of INT on the microbial community. This concern adds a layer of complexity to our interpretation of the relationship between INT reduction and the true biologically-induced oxygen consumption rates in the twilight zone. Alternatively, we attempt to recompute the conversion factor by linking *in vivo* INT reduction rates with TZR measured from BGC-float and PR + ZR approaches and derive a reduced scaling factor of 2.4 mol O_2 mol INT_F^{-1}. Applying this new factor to prior studies in the North Pacific subtropical gyre, we obtain a revised TZR of 2.5 mol C m^{-2} yr^{-1}, which is well in line with the TZR estimated by the PR + ZR approach (1.8 mol C m^{-2} yr^{-1}) (Steinberg et al., 2008). However, further studies are

Table 1
Summary of different carbon sources and demand in the South China Sea Basin.

Budget	Processes	Values (mol C m^{-2} yr^{-1})	Data Sources	Notes
Supply	Upper layer POC sinking flux	1.9 ± 1.2	Cai et al., 2008; Zhou et al., 2013; Cai et al., 2015	Measured by ^{234}Th-^{238}U disequilibrium
	DOC input	1.1 ± 0.4	Hung et al., 2007; This study	Estimated from twilight zone remineralization rate and the empirical ratio of DOC concentration to oxygen utilization rates
	Dark carbon fixation	0.7 ± 0.4	Shen et al., 2020	Measured by radioactive ^{14}C incorporation rates
	Lateral transport of POC	1.1 ± 0.2	Shen et al., 2020	Derived from the difference of POC sinking flux between theoretical and *in situ* observation from moored sediment trap
	Active transport via zooplankton migration	0.01 ± 0.02	This study	Empirically estimated from migration zooplankton biomass and allometric equations
	Sum	4.8 ± 1.3		
Demand	Twilight zone remineralization	5.7 ± 1.5	This study	Average values of BGC-float and PR + ZR estimates

POC: particulate organic carbon; DOC: dissolved organic carbon; BGC-float: biogeochemical profiling floats; PR + ZR: synthesis of prokaryotic respiration and zooplankton respiration.

needed to explore whether the large scaling factor previously reported is due to the distinct microbial assembly between the upper layer and twilight zone or systematic biases associated with the INT reduction approach itself or oxygen consumption rates derived from bottle samples.

Despite BGC-float observation and PR + ZR providing more reasonable constraints in TZR, we still need to be cautious when interpreting the data and choosing future methodologies. For example, the BGC-float approach indicates the highest vertical attenuation of TZR among the three approaches (Fig. 3b), which might reflect a reduced ability of BGC-float to capture the TZR over the depth, particularly in the horizons where TZR is close to the instrument signal-to-noise ratio of the oxygen sensor (typically 3 μmol kg^{-1}, Maurer et al. 2021). Instead, two other approaches, which rely on the respiration-relevant substrates, have a higher sensitivity, and thereby do a better job of characterizing the vertical trend of TZR. Given that the majority of respiration (>80%) occurs in the upper 400 m (Fig. 3c), the BGC-float can still robustly capture the magnitude of depth-integrated TZR. While we have used the spice as a proxy to rule out the periods affected by water mass interactions, other abiotic processes, such as the lateral diffusion and spatial heterogeneity of the preformed oxygen signal, remain unconstrained in the oxygen mass balance model (Billheimer et al. 2021; Wang and Fennel 2022). Furthermore, since many DCF processes are aerobic (Hügler and Sievert, 2011), neglecting oxygen consumption induced by DCF may result in an overestimation of respiration derived from total oxygen utilization (e.g., respiration rates estimated from BGC-float observations in our study). However, it remains a significant challenge to directly rule out the effect of DCF on oxygen change due to the lack of accurate information on the stoichiometric ratio of O_2:C alongside DCF. Nonetheless, it is worth noting that the observed O_2 consumption rates are approximately an order of magnitude higher than the DCF (Fig. 3d, Fig. 4b). In this regard, DCF seems unlikely to significantly affect the oxygen-based respiration estimates. Improving our knowledge in the parametrization of complex physics is the most straightforward solution to minimize uncertainty. The oxygen sensor has now become the most essential biogeochemical sensor carried by BGC-float (Claustre et al. 2020). The progressive increase in spatial coverage can also help partly reduce the TZR uncertainty by averaging sufficient float data to counterbalance the positive and negative biases induced by the complex physical processes (Hennon et al. 2016; Su et al. 2022).

For PR + ZR method, the largest error sources are associated with the choice in the conversation factors including LeuCF and PGE, as demonstrated by the sensitivity analysis (Fig. S7). To address this challenge, we assigned reasonable errors and ranges to LeuCF and PGE by analyzing data obtained from local and global experimental studies (see Method section). Furthermore, the agreement between TZR values from PR + ZR and BGC-float approaches, along with the carbon supply, further validates our choice of conversion factors.

4.3. Regional carbon budget

We succeed in balancing the carbon demand (the average values indicated by BGC-float observation and PR + ZR) with the carbon supply after comprehensively considering the multiple sources (Fig. 4, Table 1). Our analysis reveals that the POC sinking flux from the upper layer, determined by the ^{234}Th-^{238}U disequilibrium, accounts for only 33% of the total carbon demand, with a value of approximately 1.9 ± 1.2 mol C m^{-2} yr^{-1}. Other processes, such as DOC portion, lateral transport, and DCF, also play important roles in counterbalancing carbon demand.

Approximately 19% of the total carbon demand is met by the laterally transported POC (1.1 ± 0.2 mol C m^{-2} yr^{-1}), which is inferred from the apparent excess of POC sinking flux from sediment trap observations relative to the theoretical attenuation. The most probable source of this lateral transport POC is from the productive northern shelf through the river discharge and large-scale circulation (Liu et al. 2014; Shen et al. 2020), with enhanced transport during extreme weather conditions (Shih et al. 2019). Such an active lateral transport POC in the SCS basin has been captured by the high-resolution observations from the bio-optical sensor equipped with BGC-float (Shen et al. 2020). The researchers found that episodic elevation of POC concentration in the intermediate layer is not usually accompanied by the simultaneous increase of POC in the upper layer, implying the possible source from the lateral transport instead of vertical export. A similar mechanism of substantial shelf-to-basin POC transport has been also identified in the Barents Sea by Rogge et al. (2023) using field observations and numeric model simulations.

The portion of TZR fueled by DOC, scaled from the oxygen consumption rate and the empirical relationship between DOC and AOU, is equivalent to ~19% total carbon demand (1.1 ± 0.4 mol C m^{-2} yr^{-1}, Fig. 4, Table 1). This finding is in agreement with the previous estimates of ~20% across the global ocean (Hansell and Carlson 1998; Roshan and DeVries 2017). Notably, a unique feature of the SCS basin DOC budget is the influence from the adjacent western Pacific. Compared with the SCS basin, the western Pacific water holds a higher DOC concentration and active Kuroshio intrusion via Luzon Strait leads to a net DOC import to the SCS basin on an order of ~10 Tg C yr^{-1} in the upper 500 m over the annual cycle (Wu et al., 2015). Many studies have further confirmed that such laterally transported DOC can stimulate prokaryotic activity in the SCS basin because of elevated nutrient concentration (compared with western Pacific water) and distinct microbial community structure (Xu et al. 2018; Huang et al. 2019b; Li et al. 2021). Therefore, our estimate of DOC-associated TZR might reflect a combined contribution of downward mixing and unique lateral transport. The final source of DOC is the active flux by zooplankton diel vertical migration. In our study region, the estimated contribution of active DOC transport to the total carbon supply was found to be very limited (<1%); consistent with the recent finding (0.02 mol C m^{-2} yr^{-1}) in the same region, possibly due to the shallow depth of the deep chlorophyll maximum and strong stratification in the upper layer which impedes the amplitude of zooplankton

Table 2
The estimation of twilight zone remineralization (TZR) in the global ocean.

Method	Region	TZR (mol C m^{-2} yr^{-1})	Integrated Depth (m)	Notes	References
Oxygen utilization rate	North Atlantic Subtropical Gyre	4.5	100–1000	^{3}He-^{3}H-dating approach	Jenkins 1982
	North Atlantic Subtropical Gyre (Station BATS)	3.5	100–1000	^{3}He-^{3}H-dating approach	Stanley et al., 2012
	South China Sea basin	1.96 ± 0.2	100–1000	^{3}He-^{3}H-dating approach	Xie et al., 2021
	Sargasso Sea	4.2	100–400	BGC-float observation	Billheimer et al., 2021
	Subantarctic Southern Ocean (Drake Passage)	4.4 ± 2.9	70–600	BGC-float observation	Hennon et al., 2016
	Sargasso Sea	3.9 ± 2.3	70–600	BGC-float observation	Hennon et al., 2016
	Southern Indian Ocean	3.8 ± 1.1	70–600	BGC-float observation	Hennon et al., 2016
	Western Pacific	3.8 ± 1.8	70–600	BGC-float observation	Hennon et al., 2016
	South Pacific	3.9 ± 0.7	100–900	BGC-float observation	Martz et al., 2008
	Southern Ocean	0–4.3	100–500	BGC-float observation	Arteaga et al., 2019
	Southern Ocean	1.9–5.1	100–1000	BGC-float observation	Su et al., 2022
	South China Sea basin	5.1 ± 0.5	100–1000	BGC-float observation	This study
INT reduction	North Atlantic Subtropical Gyre	28.2 ± 4.9	200–1000	*in vitro*, R/ETS of 1.1 mol O_2/mol e^{-1}	Arístegui et al., 2020
	Northern Chilean Coast	8.8 ± 10.3	31–1000	*in vitro*, R/ETS of 0.58 mol O_2/mol e^{-1}	Fernández-Urruzola et al., 2021
	South Atlantic Gyre (Terrace Bay)	3.8	60–400	*in vitro*, R/ETS of 0.26–0.48 mol O_2/mol e^{-1}	Osma et al., 2014
	North Pacific Subtropical Gyre (Station ALOHA)	13.2	200–1000	*in vivo*, R/INT of 12.8 mol O_2/mol INT_F	Martínez-García, 2016
	South China Sea basin	30.0 ± 6.1	100–1000	*in vivo*, R/INT of 12.8 mol O_2/mol INT_F	This study
PR + ZR	North Atlantic Ocean (Porcupine Abyssal Plain)	2.6	50–1000	PGE of 8%	Giering et al., 2014
	North Pacific Subtropical Gyre (Station ALOHA)	1.8	150–1000	PGE of 1%–15%	Steinberg et al., 2008
	North Pacific Subarctic Gyre (Station K2)	5.2	150–1000	PGE of 1%–15%	Steinberg et al., 2008
	South China Sea basin	6.4 ± 3.0	100–1000	PGE of 7%	This study

BGC-float: biogeochemical profiling floats; *in vivo/in vitro* INT reduction: the reduction of a tetrazolium salt by the cellular electron transport system, depending on the respiration measurement whether in the living cell (see more details from Martínez-García et al., 2009). PR + ZR: synthesis of prokaryotic respiration and zooplankton respiration; R/ETS: oxygen consumption to electron transport system activity ratio; R/INT: oxygen consumption to INT reduction ratio; PGE: prokaryotic growth efficiency.

migration (Ge et al. 2021).

Another significant carbon source that supports the carbon demand in the SCS basin is DCF, accounting for ~12% of TZR. The magnitude of global DCF relative to the upper carbon export (here we assume this value is 10 Pg C yr^{-1}, Boyd et al. 2019) remains under debate, with estimates varying from 1–3% (Middelburg 2011; Meador et al. 2020) to 20–70% (Saxena et al. 2022). In our study region, DCF corresponds to ~30% upper layer POC flux. The relatively high oxygen concentration in the twilight zone (>70 μmol kg^{-1}, Fig S4) might provide a favorable condition to facilitate the DCF (Saxena et al. 2022). Additionally, the active DCF might be associated with the lateral transport of DOC as aforementioned. Ammonia microbial assemblages, the main contributor to DCF in the SCS basin (Zhang et al. 2020), were found to be substantially stimulated in the response to Kuroshio intrusion, as the newly NH_4^+ regeneration via decomposition of laterally transported DOC provides the substrate for the subsequent oxidation (Xu et al. 2018).

5. Conclusion

In this study, we applied three approaches, including BGC-float observation, *in vivo* INT and PR + ZR, to quantify the TZR in the SCS basin. We also compiled and reanalyzed multiple carbon supply sources from the literature to provide another independent constraint in TZR. We found that BGC-float observation and the PR + ZR provide more reliable estimates of TZR that are consistent with known carbon supply within the error range. In contrast, *in vivo* INT appears to considerably overestimate TZR, with the exact causes meriting further investigation and analysis. The regional carbon budget indicates the important contribution of multiple carbon supply pathways to sustain the high carbon demand in the twilight zone. Overall, this study provides in-depth view into methodological discrepancy and main uncertainties associated with various methods used for estimating TZR. It also emphasizes the significance of multi-disciplinary and integrated process studies in constraining biogeochemical processes in twilight zone research. However, owing to the limited dataset and techniques, our present work mainly relied on complications of historical data to close the regional budget. Future work should focus on improving spatial-temporal matching to reduce estimation uncertainties. Additionally, consideration of the seasonality of carbon supply and demand terms and their potential time lag are necessary for a more comprehensive understanding of the regional carbon cycle.

CRediT authorship contribution statement

Chao Xu: Writing – original draft, Visualization, Supervision, Software, Methodology, Formal analysis, Conceptualization. **Mingwang Xiang:** Investigation. **Bingzhang Chen:** Writing – review & editing, Conceptualization. **Yibin Huang:** Writing – review & editing, Methodology, Conceptualization. **Guoqiang Qiu:** Data curation. **Yuchen Zhang:** Writing – review & editing. **Haili Wang:** Data curation. **Bangqin Huang:** Writing – review & editing, Supervision, Resources, Project administration, Conceptualization.

Declaration of competing interest

The authors declare that they have no known competing financial interests or personal relationships that could have appeared to influence the work reported in this paper.

Data availability

Data will be made available on request.

Acknowledgments

This study was supported by the National Natural Science Foundation of China [grant numbers: 42130401, 42141002]. Yibin Huang is supported by the Fundamental Research Funds for the Central Universities [grant number: 20720240105]. We are grateful to the captain, the crew, and the scientists of the R/V *Tan Kah Kee* for their invaluable support on the experiments during the cruise. We also thank Fei Sheng for his assistance in organizing zooplankton data.

Appendix A. Supplementary data

Supplementary data to this article can be found online at https://doi.org/10.1016/j.pocean.2024.103316.

References

Al-Mutairi, H., Landry, M.R., 2001. Active export of carbon and nitrogen at Station ALOHA by diel migrant zooplankton. Deep Sea Res. Part II 48, 2083–2103.
Amano, C., Zhao, Z., Sintes, E., Reinthaler, T., Stefanschitz, J., Kisadur, M., Utsumi, M., Herndl, G.J., 2022. Limited carbon cycling due to high-pressure effects on the deep-sea microbiome. Nat. Geosci. 15, 1–7.
Anderson, L.A., Sarmiento, J.L., 1994. Redfield ratios of remineralization determined by nutrient data analysis. Global Biogeochem. Cycles 8, 65–80.
Archibald, K.M., Siegel, D.A., Doney, S.C., 2019. Modeling the impact of zooplankton diel vertical migration on the carbon export flux of the biological pump. Global Biogeochem. Cycles 33, 181–199.
Arístegui, J., Duarte, C.M., Agustí, S., Doval, M., Alvarez-Salgado, X.A., Hansell, D.A., 2002. Dissolved organic carbon support of respiration in the dark ocean. Science 298, 1967.
Arístegui, J., Montero, M.F., Hernández-Hernández, N., Alonso-González, I.J., Baltar, F., Calleja, M.L., Duarte, C.M., 2020. Variability in water-column respiration and its dependence on organic carbon sources in the Canary Current upwelling region. Front. Earth Sci. 8, 349.
Arteaga, L.A., Pahlow, M., Bushinsky, S.M., Sarmiento, J.L., 2019. Nutrient controls on export production in the Southern Ocean. Global Biogeochem. Cycles 33, 942–956.
Baños, I., Montero, M.F., Benavides, M., Arístegui, J., 2020. INT toxicity over natural bacterial assemblages from surface oligotrophic waters: implications for the assessment of respiratory activity. Microb. Ecol. 80, 237–242.
Billheimer, S.J., Talley, L.D., Martz, T.R., 2021. Oxygen seasonality, utilization rate, and impacts of vertical mixing in the eighteen degree water region of the sargasso sea as observed by profiling biogeochemical floats. Global Biogeochem. Cycles 35 e2020GB006824.
Boyd, P.W., Claustre, H., Levy, M., Siegel, D.A., Weber, T., 2019. Multi-faceted particle pumps drive carbon sequestration in the ocean. Nature 568, 327–335.
Buesseler, K.O., Boyd, P.W., Black, E.E., Siegel, D.A., 2020. Metrics that matter for assessing the ocean biological carbon pump. PNAS 117, 9679–9687.
Cai, P., Chen, W., Dai, M., Wan, Z., Wang, D., Li, Q., Tang, T., Lv, D., 2008. A high-resolution study of particle export in the southern South China Sea based on ^{234}Th:^{238}U disequilibrium. J. Geophys. Res. 113.
Cai, P., Zhao, D., Wang, L., Huang, B., Dai, M., 2015. Role of particle stock and phytoplankton community structure in regulating particulate organic carbon export in a large marginal sea. J. Geophys. Res. Oceans 120, 2063–2095.
Cassar, N., Nicholson, D., Khatiwala, S., Cliff, E., 2021. Decomposing the oxygen signal in the ocean interior: Beyond decomposing organic matter. Geophys. Res. Lett. 48 e2021GL092621.
Chai, F., Johnson, K.S., Claustre, H., Xing, X., Wang, Y., Boss, E., Riser, S., Fennel, K., Schofield, O., Sutton, A., 2020. Monitoring ocean biogeochemistry with autonomous platforms. Nat. Rev. Earth Environ. 1, 315–326.
Chen, Y.-l.L., 2005. Spatial and seasonal variations of nitrate-based new production and primary production in the South China Sea. Deep Sea Res. Part I 52, 319–340.
Chen, C.-T.-A., Wang, S.-L., Wang, B.-J., Pai, S.-C., 2001. Nutrient budgets for the South China Sea basin. Mar. Chem. 75, 281–300.
Chisholm, S.W., 2000. Stirring times in the Southern Ocean. Nature 407, 685–686.
Claustre, H., Johnson, K.S., Takeshita, Y., 2020. Observing the global ocean with biogeochemical-Argo. Ann. Rev. Mar. Sci. 12, 23–48.
Dai, M., Su, J., Zhao, Y., Hofmann, E.E., Cao, Z., Cai, W.-J., Gan, J., Lacroix, F., Laruelle, G.G., Meng, F., Müller, J.D., Regnier, P.A.G., Wang, G., Wang, Z., 2022. Carbon fluxes in the Coastal Ocean: Synthesis, boundary processes and future trends. Annu. Rev. Earth Planet. Sci. 50, 593–626.
del Giorgio, P.A., Cole, J.J., 1998. Bacterial growth efficiency in natural aquatic systems. Annu. Rev. Ecol. Syst. 29, 503–541.
del Giorgio, P.A., Williams, P., 2005. Respiration in aquatic ecosystems. OUP Oxford.
Ducklow, H.W., Doney, S.C., 2013. What is the metabolic state of the oligotrophic ocean? A debate. Ann. Rev. Mar. Sci. 5, 525–533.
Emerson, S., 2014. Annual net community production and the biological carbon flux in the ocean. Global Biogeochem. Cycles 28, 14–28.
Feely, R.A., Sabine, C.L., Schlitzer, R., Bullister, J.L., Mecking, S., Greeley, D., 2004. Oxygen utilization and organic carbon remineralization in the upper water column of the Pacific Ocean. J. Oceanogr. 60, 45–52.
Fernández-Urruzola, I., Ulloa, O., Glud, R.N., Pinkerton, M.H., Schneider, W., Wenzhöfer, F., Escribano, R., 2021. Plankton respiration in the Atacama Trench region: Implications for particulate organic carbon flux into the hadal realm. Limnol. Oceanogr. 66, 3134–3148.
Gaarder, T., 1927. Investigations of the production of plankton in the Oslo Fjord. Rapports et Proces-verbaux des Reunions. Conseil International pour l'Exploration de la Mer 42, 1–48.
García-Martín, E.E., Aranguren-Gassis, M., Karl, D.M., Martínez-García, S., Robinson, C., Serret, P., Teira, E., 2019. Validation of the in vivo iodo-nitro-tetrazolium (INT) salt reduction method as a proxy for plankton respiration. Front. Mar. Sci. 6, 220.
Ge, R., Chen, H., Zhuang, Y., Liu, G., 2021. Active carbon flux of mesozooplankton in South China Sea and Western Philippine Sea. Front. Mar. Sci. 8, 697743.
Giering, S.L.C., Evans, C., 2022. Overestimation of prokaryotic production by leucine incorporation—and how to avoid it. Limnol. Oceanogr. 67 (3), 726–738.
Giering, S.L.C., Sanders, R., Lampitt, R.S., Anderson, T.R., Tamburini, C., Boutrif, M., Zubkov, M.V., Marsay, C.M., Henson, S.A., Saw, K., Cook, K., Mayor, D.J., 2014. Reconciliation of the carbon budget in the ocean's twilight zone. Nature 507, 480–483.
Guo, C., Ke, Y., Chen, B., Zhang, S., Liu, H., 2022. Making comparable measurements of bacterial respiration and production in the subtropical coastal waters. Mar. Life Sci. Technol. 4, 414–427.
Hansell, D.A., Carlson, C.A., 1998. Net community production of dissolved organic carbon. Global Biogeochem. Cycles 12, 443–453.
He, X., Liang, C., Yang, Y., Chen, G., Shang, X., He, X., Tong, P., 2022. Vertical multiple-layer structure of temperature and turbulent diffusivity in the South China Sea. Acta Oceanol. Sin. 41, 14–21.
Hennon, T.D., Riser, S.C., Mecking, S., 2016. Profiling float-based observations of net respiration beneath the mixed layer. Global Biogeochem. Cycles 30, 920–932.
Henson, S.A., Sanders, R., Madsen, E., 2012. Global patterns in efficiency of particulate organic carbon export and transfer to the deep ocean. Global Biogeochem, Cycles, p. 26.
Huang, Y., Yang, B., Chen, B., Qiu, G., Wang, H., Huang, B., 2018. Net community production in the South China Sea Basin estimated from in situ O2 measurements on an Argo profiling float. Deep Sea Res. Part I 131, 54–61.
Huang, Y., Chen, B., Huang, B., Zhou, H., Yuan, Y., 2019a. Potential overestimation of community respiration in the western Pacific boundary ocean: What causes the putative net heterotrophy in oligotrophic systems? Limnol. Oceanogr. 64, 2202–2219.
Huang, Y., Laws, E., Chen, B., Huang, B., 2019b. Stimulation of heterotrophic and autotrophic metabolism in the mixing zone of the Kuroshio current and northern South China Sea: Implications for export production. J. Geophys. Res. Biogeosci. 124, 2645–2661.
Huang, Y., Fassbender, A.J., Long, J.S., Johannessen, S., Bernardi Bif, M., 2022. Partitioning the export of distinct biogenic carbon pools in the Northeast Pacific Ocean using a biogeochemical profiling float. Global Biogeochem. Cycles. 36, e2021GB007178.
Hügler, M., Sievert, S.M., 2011. Beyond the Calvin cycle: autotrophic carbon fixation in the ocean. Ann. Rev. Mar. Sci. 3, 261–289.
Hung, J.-J., Wang, S.-M., Chen, Y.-L., 2007. Biogeochemical controls on distributions and fluxes of dissolved and particulate organic carbon in the Northern South China Sea. Deep Sea Res. Part II 54, 1486–1503.
Ikeda, T., 1985. Metabolic rates of epipelagic marine zooplankton as a function of body mass and temperature. Mar. Biol. 85, 1–11.
Ikeda, T., Kanno, Y., Ozaki, K., Shinada, A., 2001. Metabolic rates of epipelagic marine copepods as a function of body mass and temperature. Mar. Biol. 139, 587–596.
Jenkins, W.J., 1982. Oxygen utilization rates in North Atlantic subtropical gyre and primary production in oligotrophic systems. Nature 300, 246–248.
Kelly, T.B., Knapp, A.N., Landry, M.R., Selph, K.E., Shropshire, T.A., Thomas, R.K., Stukel, M.R., 2021. Lateral advection supports nitrogen export in the oligotrophic open-ocean Gulf of Mexico. Nat. Commun. 12, 235.
Klymak, J.M., Crawford, W., Alford, M.H., MacKinnon, J.A., Pinkel, R., 2015. Along-isopycnal variability of spice in the North Pacific. J. Geophys. Res. Oceans 120, 2287–2307.
Koeve, W., Kähler, P., 2016. Oxygen utilization rate (OUR) underestimates ocean respiration: A model study. Global Biogeochem. Cycles 30, 1166–1182.
Lacour, L., Briggs, N., Claustre, H., Ardyna, M., Dall'Olmo, G., 2019. The Intraseasonal Dynamics of the Mixed Layer Pump in the Subpolar North Atlantic Ocean: A Biogeochemical-Argo Float Approach. Global Biogeochem. Cycles 33, 266–281.
Lahajnar, N., Wiesner, M.G., Gaye, B., 2007. Fluxes of amino acids and hexosamines to the deep South China Sea. Deep Sea Res. 1. Oceanogr. Res. Pap. 54, 2120–2144.
Laws, E.A., D'Sa, E., Naik, P., 2011. Simple equations to estimate ratios of new or export production to total production from satellite-derived estimates of sea surface temperature and primary production. Limnol. Oceanogr. Methods 9, 593–601.

Li, T., Bai, Y., He, X., Xie, Y., Chen, X., Gong, F., Pan, D., 2018. Satellite-based estimation of particulate organic carbon export in the northern South China Sea. J. Geophys. Res. Oceans 123, 8227–8246.
Li, X., Wu, K., Gu, S., Jiang, P., Li, H., Liu, Z., Dai, M., 2021. Enhanced biodegradation of dissolved organic carbon in the western boundary Kuroshio Current when intruded to the marginal South China Sea. J. Geophys. Res. Oceans 126 e2021JC017585.
Liu, K.-K., Chao, S.-Y., Shaw, P.-T., Gong, G.-C., Chen, C.-C., Tang, T.Y., 2002. Monsoon-forced chlorophyll distribution and primary production in the South China Sea: observations and a numerical study. Deep Sea Res. 1. Oceanogr. Res. Pap. 49, 1387–1412.
Liu, J., Clift, P.D., Yan, W., Chen, Z., Chen, H., Xiang, R., Wang, D., 2014. Modern transport and deposition of settling particles in the northern South China Sea: sediment trap evidence adjacent to Xisha Trough. Deep Sea Res. 1. Oceanogr. Res. Pap. 93, 145–155.
Long, M.C., Deutsch, C., Ito, T., 2016. Finding forced trends in oceanic oxygen. Global Biogeochem. Cycles 30, 381–397.
Maldonado, F., Packard, T.T., Gómez, M., 2012. Understanding tetrazolium reduction and the importance of substrates in measuring respiratory electron transport activity. J. Exp. Mar. Biol. Ecol. 434, 110–118.
Martínez-García, S., 2016. Microbial respiration in the mesopelagic zone at Station ALOHA. Limnol. Oceanogr. 62, 320–333.
Martínez-García, S., Fernández, E., Aranguren-Gassis, M., Teira, E., 2009. In vivo electron transport system activity: a method to estimate respiration in natural marine microbial planktonic communities. Limnol. Oceanogr. Methods 7, 459–469.
Martz, T.R., Johnson, K.S., Riser, S.C., 2008. Ocean metabolism observed with oxygen sensors on profiling floats in the South Pacific. Limnol. Oceanogr. 53, 2094–2111.
Maurer, T.L., Plant, J.N., Johnson, K.S., 2021. Delayed-mode quality control of oxygen, nitrate, and pH data on SOCCOM biogeochemical profiling floats. Front. Mar. Sci. 8, 683207.
Meador, T.B., Schoffelen, N., Ferdelman, T.G., Rebello, O., Khachikyan, A., Könneke, M., 2020. Carbon recycling efficiency and phosphate turnover by marine nitrifying archaea. Sci. Adv. 6, eaba1799.
Middelburg, J.J., 2011. Chemoautotrophy in the ocean. Geophys. Res, Lett, p. 38.
Ning, X.-R., Chai, F., Xue, H., Cai, Y., Liu, C., Shi, J., 2004. Physical-biological oceanographic coupling influencing phytoplankton and primary production in the South China Sea. J. Geophys. Res. 109.
Osma, N., Fernández-Urruzola, I., Packard, T.T., Postel, L., Gómez, M., Pollehne, F., 2014. Short-term patterns of vertical particle flux in northern Benguela: a comparison between sinking POC and respiratory carbon consumption. J. Mar. Syst. 140, 150–162.
R Core Team, 2021. R: A language and environment for statistical computing. Austria, Vienna.
Ran, L., Chen, J., Wiesner, M.G., Ling, Z., Lahajnar, N., Yang, Z., Li, H., Hao, Q., Wang, K., 2015. Variability in the abundance and species composition of diatoms in sinking particles in the northern South China Sea: Results from time-series moored sediment traps. Deep Sea Res. Part II 122, 15–24.
Rogge, A., Janout, M., Loginova, N., Trudnowska, E., Hörstmann, C., Wekerle, C., Oziel, L., Schourup-Kristensen, V., Ruiz-Castillo, E., Schulz, K., 2023. Carbon dioxide sink in the Arctic Ocean from cross-shelf transport of dense Barents Sea water. Nat. Geosci. 16, 82–88.
Roshan, S., DeVries, T., 2017. Efficient dissolved organic carbon production and export in the oligotrophic ocean. Nat. Commun. 8, 1–8.
Saxena, H., Sahoo, D., Nazirahmed, S., Rai, D.K., Khan, M.A., Sharma, N., Kumar, S., Singh, A., 2022. Contribution of carbon fixation towards carbon sink in the ocean twilight zone. Geophys. Res. Lett. 49, e2022GL099044.
Shang, X.-D., Liang, C.-R., Chen, G.-Y., 2017. Spatial distribution of turbulent mixing in the upper ocean of the South China Sea. Ocean Sci. 13, 503–519.
Shen, J., Jiao, N., Dai, M., Wang, H., Qiu, G., Chen, J., Li, H., Kao, S.-J., Yang, J.-Y.-T., Cai, P., 2020. Laterally transported particles from margins serve as a major carbon and energy source for dark ocean ecosystems. Geophys. Res. Lett. 47 e2020GL088971.
Shih, Y.-Y., Lin, H.-H., Li, D., Hsieh, H.-H., Hung, C.-C., Chen, C.-T.-A., 2019. Elevated carbon flux in deep waters of the South China Sea. Sci. Rep. 9, 1496.
Smith, D.C., Azam, F., 1992. A simple, economical method for measuring bacterial protein synthesis rates in seawater using 3H-leucine. Mar. Microb. Food Webs 6, 107–114.
Smith, T.P., Clegg, T., Bell, T., Pawar, S., 2021. Systematic variation in the temperature dependence of bacterial carbon use efficiency. Ecol. Lett. 24, 2123–2133.
Stanley, R.H.R., Doney, S.C., Jenkins, W.J., Lott, I.D.E.I.I., 2012. Apparent oxygen utilization rates calculated from tritium and helium-3 profiles at the Bermuda Atlantic Time-series Study site. Biogeosciences 9, 1969–1983.
Steinberg, D.K., Carlson, C.A., Bates, N.R., Goldthwait, S.A., Madin, L.P., Michaels, A.F., 2000. Zooplankton vertical migration and the active transport of dissolved organic and inorganic carbon in the Sargasso Sea. Deep Sea Res. Part I 47, 137–158.
Steinberg, D.K., Van Mooy, B.A.S., Buesseler, K.O., Boyd, P.W., Kobari, T., Karl, D.M., 2008. Bacterial vs. zooplankton control of sinking particle flux in the ocean's twilight zone. Limnol. Oceanogr. 53, 1327–1338.
Su, J., Schallenberg, C., Rohr, T., Strutton, P.G., Phillips, H.E., 2022. New estimates of southern ocean annual net community production revealed by BGC-Argo floats. Geophys. Res. Lett. 49 e2021GL097372.
Tiano, L., Garcia-Robledo, E., Dalsgaard, T., Devol, A.H., Ward, B.B., Ulloa, O., Canfield, D.E., Revsbech, N.P., 2014. Oxygen distribution and aerobic respiration in the north and south eastern tropical Pacific oxygen minimum zones. Deep Sea Res. 1. Oceanogr. Res. Pap. 94, 173–183.
Wang, B., Fennel, K., 2022. Biogeochemical-Argo data suggest significant contributions of small particles to the vertical carbon flux in the subpolar North Atlantic. Limnol. Oceanogr. 67, 2405–2417.
Wu, K., Dai, M., Chen, J., Meng, F., Li, X., Liu, Z., Du, C., Gan, J., 2015. Dissolved organic carbon in the South China Sea and its exchange with the Western Pacific Ocean. Deep Sea Res. Part II 122, 41–51.
Xie, T., Newton, R., Schlosser, P., Guo, L., Wang, L., Huang, T., Li, Y., Wang, Z., Dai, M., 2021. Apparent oxygen utilization rates based on tritium-helium dating in the South China Sea: Implications for export production. Deep Sea Res. Part I 177, 103620.
Xu, M.N., Zhang, W., Zhu, Y., Liu, L., Zheng, Z., Wan, X.S., Qian, W., Dai, M., Gan, J., Hutchins, D.A., 2018. Enhanced ammonia oxidation caused by lateral Kuroshio intrusion in the boundary zone of the northern South China Sea. Geophys. Res. Lett. 45, 6585–6593.
Zhang, Y., Qin, W., Hou, L., Zakem, E.J., Wan, X., Zhao, Z., Liu, L., Hunt, K.A., Jiao, N., Kao, S.-J., Tang, K., Xie, X., Shen, J., Li, Y., Chen, M., Dai, X., Liu, C., Deng, W., Dai, M., Ingalls, A.E., Stahl, D.A., Herndl, G.J., 2020. Nitrifier adaptation to low energy flux controls inventory of reduced nitrogen in the dark ocean. PNAS 117, 4823–4830.
Zhang, W.-Z., Wang, H., Chai, F., Qiu, G., 2016. Physical drivers of chlorophyll variability in the open South China Sea. J. Geophys. Res. Oceans 121, 7123–7140.
Zhou, K., Dai, M., Kao, S.-J., Wang, L., Xiu, P., Chai, F., Tian, J., Liu, Y., 2013. Apparent enhancement of ^{234}Th-based particle export associated with anticyclonic eddies. Earth Planet. Sci. Lett. 381, 198–209.